Nanoscale

PAPER

View Article Online
View Journal | View Issue

Cite this: *Nanoscale*, 2025, **17**, 16784

In search of the smoothest nanoparticle surface: diffusion and mobility on Ag clusters

Nicolò Canestrari, Riccardo Ferrando and Diana Nelli *

Surface diffusion is the key atomic process in nanoparticle growth. Regular shapes and low-defect surfaces can only be obtained if the deposited atoms are able to move over the entire surface of the nanoparticle—something that may be hindered by the presence of edges separating adjacent facets. Edge crossing is the rate-limiting step for adatom diffusion on nanoparticle surfaces and, consequently, edges of different sharpness are expected to affect diffusion processes differently. Here, we investigate this problem in the case of a silver adatom diffusing on top of nanoparticles with different geometric shapes: tetrahedron, octahedron, Mackay icosahedron, and chiral icosahedron. All structures have close-packed (111) facets—on which diffusion is very fast—separated by edges of different types. Using molecular dynamics simulations, we identify the most relevant edge-crossing processes and estimate their activation barriers. Our results clearly show that the geometrical shape of the nanoparticle strongly influences the inter-facet diffusion of atoms, affecting the energy barriers associated with edge-crossing processes. Jump and exchange diffusion barriers depend on the edge sharpness in opposite ways, so that—interestingly—the smoothest surfaces for adatom diffusion are both the sharpest (the tetrahedron) and the most rounded (the chiral icosahedron). Our results for Ag clusters are expected to hold for other fcc metals as well.

Received 29th April 2025,
Accepted 25th June 2025

DOI: 10.1039/d5nr01752a

rsc.li/nanoscale

1 Introduction

Diffusion of adatoms on metal surfaces is the elementary process underlying the growth of metallic materials. The characteristic time scales of adatom diffusion strongly influence the quality of the growth process and of the resulting product. If deposited adatoms can diffuse rather freely, growth proceeds regularly and smooth final surfaces are obtained; otherwise, metal surfaces tend to be irregular and disordered.[1]

A paradigmatic example of a metallic object grown by atom deposition is the thin film.[2] A thin film consists of a few flat atomic layers grown on top of each other in a highly controlled manner. The elementary atomic mechanism underlying such a growth process is the diffusion of individual adatoms on the metal surface. Other processes may occur, such as the diffusion of small clusters or the concerted displacement of fully developed islands, but these are expected, in many cases, to be less relevant compared to single-atom motion.[3] As such, the diffusion of individual adatoms on metal surfaces has been widely investigated in the last decades, through both experimental and theoretical/computational techniques.[4–19]

Different kinds of diffusion processes have been studied: diffusion on defect-free flat surfaces with well-defined crystallographic orientations ((111), (100), and (110) are the most relevant for fcc and bcc metals);[5–9,20] diffusion on surfaces with defects or imperfections, such as steps, kinks, or vacancies;[10,12–14] homo-diffusion, in which the diffusing adatom and the metal surface belong to the same species;[7,10,12] hetero-diffusion, in which the adatom and the surface belong to different species;[6,9,21] jump diffusion, where the adatom moves from one adsorption site to a nearby one;[6,8,15] and exchange diffusion, in which the adatom enters the metal surface by exchanging positions with a surface atom, which then moves to a nearby adsorption site.[7,9,10,12,13,15,16] Diffusion coefficients and activation barriers have been estimated,[15,22] allowing researchers to identify the conditions under which smooth, layer-by-layer growth can be achieved.

Nanoparticles are another type of metallic object that can be grown by atom deposition.[23–25] Again, a regular overall shape and a smooth surface can be achieved provided that the diffusion of the deposited atoms is sufficiently fast—*i.e.*, if the adatoms can move over the entire surface of the nanoparticle without getting stuck in trap sites.[26–30] In this case, the situation is considerably more complex than in thin film growth, due to the presence of edges separating adjacent flat facets of the nanoparticle.

Dipartimento di Fisica, Università di Genova, Via Dodecaneso 33, 16146 Genova, Italy. E-mail: diana.nelli@edu.unige.it

The presence of edges renders the diffusion problem truly three-dimensional. When an atom diffuses within a facet, the behavior closely resembles that observed on an infinite planar surface. However, when the atom moves from one facet to another, the edge between them introduces an additional energy barrier, typically much higher than that associated with diffusion within the same facet.[26,27,30–34] Therefore, even when intra-facet diffusion is fully activated, the adatom may be unable to easily cross the edge, and may remain confined to a single facet for extended periods. Edge crossing thus becomes a rate-limiting step in surface diffusion on nanoparticles, and a key factor limiting the regularity and smoothness of nanoparticle growth.

Here, we study the diffusion of an Ag adatom on the surface of nanoparticles with Ag close-packed facets, *i.e.*, with (111) crystallographic orientation. Diffusion on the (111) surface is very fast, due to the low adsorption energy at three-fold adsorption sites and the small corrugation of the surface. This fast intra-facet diffusion allows us to isolate the effect of edges on overall surface diffusion. Specifically, we aim to investigate how different types of edges separating adjacent (111) facets affect diffusion pathways and the corresponding activation barriers. To this end, we employ molecular dynamics (MD) simulations to reproduce the diffusion of a single Ag atom on the surface of nanoparticles of similar size but different geometric shapes, and we evaluate both static and dynamic energy barriers for the most relevant edge-crossing processes. In Fig. 1, we show the nanoparticle shapes considered in our work. These are the three regular polyhedra (also known as Platonic solids) with triangular faces: the *tetrahedron*, the *octahedron*, and the *icosahedron*. As shown in Fig. 1 (d–g), atoms can be assembled into nanoparticles with these symmetries, exposing close-packed facets with (111) orientation. For the icosahedron, different atomic assemblies are possible, as discussed in detail in ref. 35. Here, we consider the well-known Mackay icosahedron[36] (Fig. 1(f)) and an icosahedron in which the surface atoms have a chiral arrangement (Fig. 1(e)). As explained in ref. 35, chiral icosahedral surfaces are stabilized by the presence of atoms with smaller atomic radius in the inner shells, with an appropriate size mismatch. In this case, the icosahedron consists of four inner Mackay shells of Ni atoms, surrounded by two chiral Ag shells.

The dihedral angles (angles between two adjacent facets) of the tetrahedron, octahedron, and icosahedron are70.5°, 109.5°, and138.2°, respectively. These values give an indication of the sharpness of the nanoparticle edges: the tetrahedron has the sharpest edges, followed by the octahedron, and then the Mackay icosahedron. The chiral icosahedron differs significantly in this respect, as well-defined edges cannot be clearly identified. In the other structures, the nanoparticle edges correspond exactly to the geometric edges—*i.e.*, straight lines connecting nearby vertices; in other words, adjacent vertices are joined by straight rows of atoms (see Fig. 1(h–l)). In contrast, in the chiral icosahedral surface, atoms are located either on one side or the other of the geometric edge, so that a true nanoparticle edge does not exist (see Fig. 1(m)). As we will show, this peculiar feature strongly affects adatom diffusion on the nanoparticle surface.

Nanoparticles with the geometric shapes shown in Fig. 1 have been experimentally observed for several fcc metals, including silver. Computer simulations have demonstrated that these shapes are stable over a wide range of temperatures and, although they may not correspond to the lowest-energy configuration, they can dynamically form during synthesis as a result of specific growth processes.

In the following, we compare the diffusion processes and time scales on the surface of the four different nanoparticles shown in Fig. 1(d–g). Nanoparticle sizes are in the range of1.5–2.3 nm, corresponding to 560, 670, 923, and 833 atoms in the tetrahedron, octahedron, Mackay icosahedron, and chiral icosahedron, respectively. Our ultimate goal is to classify the nanoparticle structures in terms of *smoothness—i.e.*, to determine which nanoparticle shape is associated with the lowest diffusion barriers and, consequently, with the fastest diffusion of deposited atoms.

2 Methods

The interactions between atoms are modeled using an atomistic potential developed by Gupta and Rosato *et al.*,[37,38] based on the second-moment approximation of the tight-binding model. The interaction parameters are taken from previous studies on Ag and core–shell Ni@Ag nanoparticles.[39,40] This model has been successfully employed in the study of adatom self-diffusion on Ag surfaces of different crystallographic orientations.[15,41] The calculated energy barrier for jump diffusion on the (100) surface is 0.43 eV, in very good agreement with experimental data (0.40 eV (ref. 42) and 0.38 eV (ref. 43)). For other diffusion processes—such as exchange diffusion on the (100) surface and jump or exchange diffusion on the (110) surface—experimental data are not available. In these cases, the calculated energy barriers have been compared to those obtained from other computational methods (Embedded Atom Model and Density Functional Theory[15,44]), with good agreement in all cases. For example, the energy barrier for in-channel jump diffusion on the (110) surface is 0.28 eV according to our model, in excellent agreement with the result of recent DFT calculations (0.29 eV).[44] As for jump diffusion on the (111) surface, the calculated energy barrier is 0.068 eV,[41] in good agreement with the Embedded Atom Model result (0.055 eV (ref. 45)), and only slightly lower than both the experimental estimate (0.097 ± 0.010 eV (ref. 46)) and the DFT calculation (0.081 eV (ref. 47)).

MD simulations are performed using our own code: the equations of motion are integrated using the velocity-Verlet algorithm with a time step of 5 fs, while temperature is kept constant using an Andersen thermostat. This protocol is the same as that used in previous studies to interpret gas-phase growth experiments.[24,48,49] In all MD simulations, a single Ag atom is placed on the surface of a magic-size, defect-free Ag or Ni@Ag nanoparticle and allowed to diffuse freely.

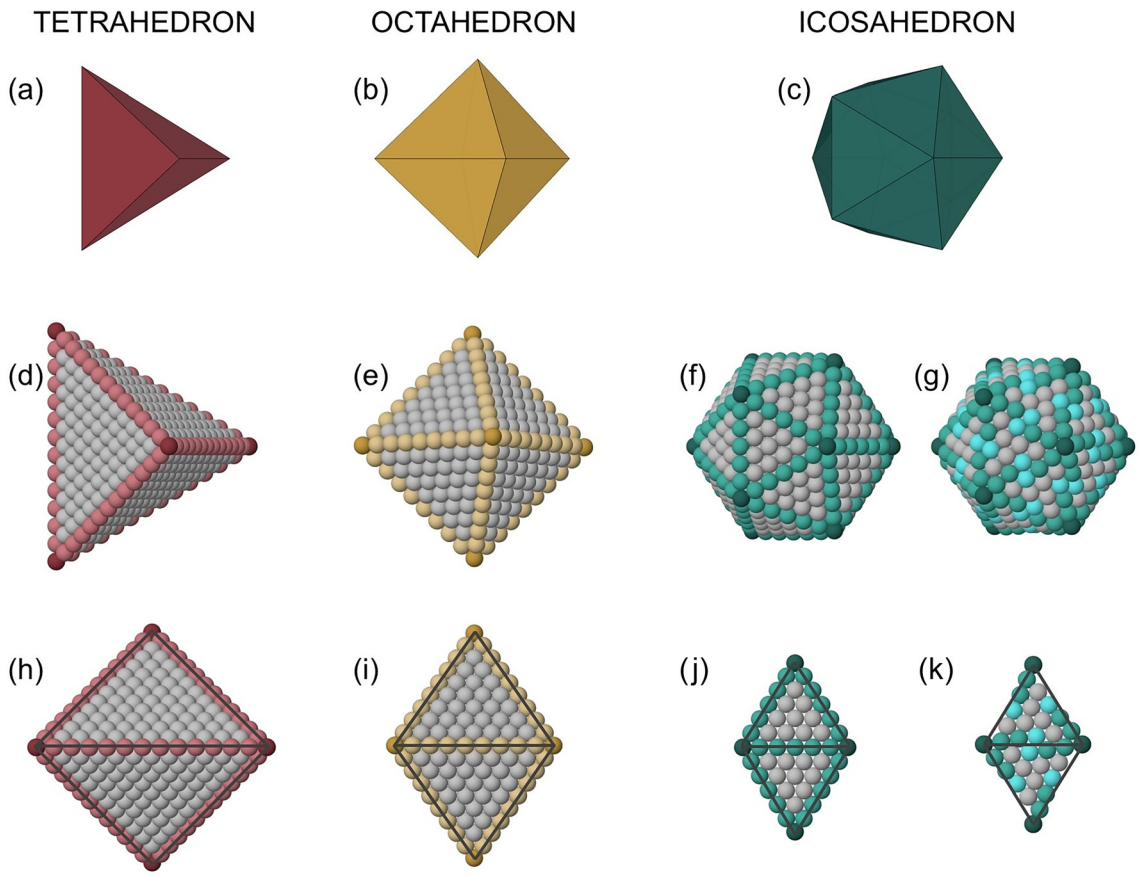

Fig. 1 Nanoparticle structures with closed-packed surface. Platonic solids with triangular faces: (a) tetrahedron; (b) octahedron; and (c) icosahedron. Nanoparticle structures corresponding to the Platonic solids considered in this work: (d) tetrahedral nanoparticle made of 560 Ag atoms; (e) octahedral nanoparticle made of 670 Ag atoms; (f) icosahedral nanoparticle made of 923 Ag atoms with Mackay arrangement; (g) icosahedral nanoparticle made of 309 Ni atoms with Mackay arrangement, surrounded by to chiral shells made of 524 Ag atoms. (h) Tetrahedral, (i) octahedral and (j) Mackay icosahedral edge. (k) Two adjacent facets of the chiral icosahedral surface. In this case, the geometric edge does not correspond to a nanoparticle edge, *i.e.* adjacent vertices are not connected by a straight row of atoms. In (d–k) atoms are colored according to their local symmetry, identified by the Common Neighbour Analysis (CNA). In (d–f), dark/light red, yellow and green identify atoms in tetrahedral, octahedral and icosahedral vertices/edges, respectively, whereas atoms in (111) triangular facets are coloured in grey. For the chiral icosahedron in (g), the CNA map is more complex, as four types of non-equivalent surface sites can be identified: vertices (dark green), edge-like (light green), (111) (grey) and bridges between edge-like sites (light blue).

The temperature range considered depends on the size and shape of the nanoparticle, and is chosen so that a large number of diffusion events can be observed while preserving the nanoparticle's perfect original symmetry (*i.e.*, no displacement of vertex or near-vertex atoms).

Potential energy barriers for the most relevant elementary diffusion processes observed during constant-temperature MD simulations are evaluated using the drag method.[50] This method is widely used for estimating energy barriers in simple processes where the transition path can be reasonably guessed. A drag coordinate connecting the initial and final states of the process is defined and incrementally increased to drag the system from the initial to the final configuration. At each step, the drag coordinate is held fixed while the other degrees of freedom are relaxed using an energy minimization procedure. The energy profile along the drag coordinate is then used to identify the saddle point and the corresponding energy barrier. In our case, the drag coordinate is the straight line connecting the two adsorption sites before and after Ag adatom diffusion. The adatom is moved stepwise along this line, and the entire nanoparticle is relaxed at each step. In addition to constraining the drag coordinate, we fix a number of atoms in the nanoparticle during relaxation to prevent the system from rotating or relaxing into one of the potential energy minima (*i.e.*, configurations with the adatom in either of the two adsorption sites). Fixed atoms are chosen far from the diffusing adatom to avoid perturbing the diffusion process. Specifically, we fix a small group of atoms near the geometric center of the nanoparticle (13, 6, and 4 atoms for the icosahedron, octahedron, and tetrahedron, respectively), as well as all vertex atoms except those closest to the diffusing atom. We tested different configurations and verified that the resulting energy barriers do not depend on the specific choice of fixed atoms.

Relaxation is performed using quenched molecular dynamics (qMD),[51] a variant of the traditional technique in which the dynamics are altered to bring the system to the nearest local minimum. Specifically, velocities that point opposite to the forces (*i.e.*, away from the minimum) are set to zero. The initial temperature of the qMD simulations is 300 K, and it gradually decreases during the simulation due to velocity damping as the system approaches the minimum. Compared to other local minimization algorithms commonly used in similar systems (such as the BFGS algorithm[52]), qMD is slower, but it offers significant advantages for our specific application. Most notably, it is straightforward to implement and naturally allows for constrained minimization, where selected degrees of freedom can be fixed during the relaxation. In our case, the constrained coordinate is the drag coordinate.

3 Adsorption sites on nanoparticle facets and intra-facet diffusion

In perfect 2D flat surfaces with (111) crystallographic orientation, all adsorption sites are equivalent, and therefore the same activation barrier is associated with adatom diffusion between any pair of neighboring sites. As a result, a deposited adatom diffuses randomly on the metal surface without any preferential direction, with the diffusion rate depending on the activation barrier and the surface temperature. The presence of defects, such as steps and vacancies, modifies this simple picture, as inequivalent sites and diffusion barriers come into play. In 3D nanoparticles, the finite size of the (111) facets introduces inequivalences between three-fold adsorption sites even in the absence of defects. Adsorption site energies vary depending on their position within the facet, particularly with respect to their proximity to edges and vertices.

We have mapped all possible adsorption sites on the triangular facets of the nanoparticles shown in Fig. 1(d–g). The results are presented in Fig. 2, where the sites are colored according to the total potential energy of the system (nanoparticle + adatom).

In all cases, adsorption sites are three-fold hollow sites, in either fcc or hcp stacking with respect to the underlying atomic layers. Bridge and top sites, where the adatom is coordinated with two and on surface atoms, respectively, are not stable adsorption sites. As we will see, bridge sites are occasionally encountered along diffusion pathways, whereas top sites are never encountered due to their very high energy, consistently with previous studies on adatom diffusion on Ag (111) surfaces.[41]

The lowest-energy sites are located near the nanoparticle vertices, and the energy increases as one moves toward the center of the facets. This is due to a better relaxation of surface atoms near the edges and vertices, where atomic coordination is lower than at the facet center.[53] We note that the energy difference between the highest- and lowest-energy adsorption sites varies across the four structures. The chiral and Mackay icosahedra both exhibit a small energy variation of 0.02–0.03 eV, while the octahedron and tetrahedron show larger differences, of 0.10 and 0.06 eV, respectively.

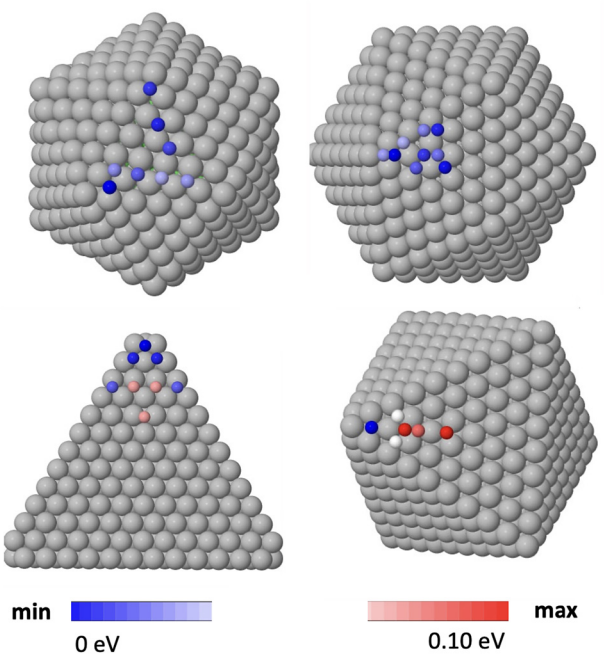

Fig. 2 Energy differences between different adatom positions. In order from the up and left: chiral icosahedron, Mackay icosahedron, tetrahedron and octahedron. In the tetrahedron, the four vertices are removed, as in the MD simulations. For each structure, we show the inequivalent adsorption sites (small spheres on the nanoparticle surface), coloured according to their energy difference from the most favourable site on that structure.

Our results show that diffusion within a (111) nanoparticle facet is not random as in its 2D counterpart, since the adatom is expected to spend more time in the most thermodynamically stable sites—*i.e.*, those of lowest energy. This behavior is consistent with our MD simulations. When the adatom diffuses on the surface of the octahedron and tetrahedron, we observe a strong preference for sites near the vertices and edges, while sites near the facet center are disfavored. In the case of the chiral and Mackay icosahedra, where adsorption sites are closer in energy, our simulations show that adatom positioning near the vertices or edges is only slightly more favorable than at the facet center.

The occupancy behavior observed in MD simulations can also be interpreted from a kinetic perspective, by analyzing the asymmetry in the diffusion energy barriers between neighboring sites. Due to the inequivalence of adsorption sites across the surface, the diffusion barrier for moving from an inner facet site to an edge site is typically lower than that for the reverse process. As a result, once the adatom reaches an edge or vertex region, it tends to become transiently trapped there, spending more time before overcoming the higher barrier required to return toward the facet center.

Barriers for moving from the center of a facet toward the edges are quite low—in the range of 0.04–0.06 eV—which is

compatible with the energy barrier for diffusion on the 2D (111) silver surface, as evaluated using the same model and method.[41]

4 MD simulations of adatom diffusion

The diffusion of the Ag adatom on the nanoparticle surfaces is simulated using MD. Simulation temperatures are high enough to ensure that the adatom diffuses over the entire nanoparticle surface, *i.e.*, that a significant number of edge-crossing events can be observed within a simulation time of a few hundred nanoseconds. However, if the temperature is too high, we observe some events that may interfere with the adatom's diffusion. The most common is the detachment of low-coordinated vertex atoms, which become adatoms themselves and begin to diffuse on the nanoparticle surface. These atoms may interact with the initial adatom, forming small islands on the surface and thereby hindering diffusion; moreover, the adatom may reach an empty vertex site and become trapped there. To avoid such events, we impose an upper limit on the simulation temperature.

The temperature range depends on the nanoparticle structure: it is 275–400 K for the chiral icosahedron, 350–450 K for the Mackay icosahedron, 275–350 K for the octahedron, and 75–150 K for the tetrahedron. In the case of the tetrahedron, vertex atoms are very poorly coordinated, having only three first-neighbor bonds—the same as an isolated atom on a (111) surface. As a result, in our simulations, they detach at any temperature, making it impossible to study the diffusion of a single adatom. Therefore, we simulate adatom diffusion on a tetrahedral nanoparticle in which the four vertex atoms have been removed (see Fig. 2). Some edge atoms also detach if the simulation temperature is too high. For this reason, we had to run simulations at much lower temperatures compared to the other structures. Nonetheless, we were able to collect enough events for statistical analysis.

Our simulations reveal different types of inter-facet diffusion pathways and edge-crossing processes. In the octahedron and tetrahedron, edge crossing always occurs *via* an exchange mechanism. Two atoms are involved in the process: the adatom and one of the edge atoms. The adatom enters the edge and displaces the edge atom, which then becomes an adatom on the adjacent facet.

In the Mackay icosahedron, jump processes are the most common. Only the adatom is involved: it moves from one facet to an adjacent one by "climbing" the edge that separates them. Exchange processes are sometimes observed, but they are only activated at the highest simulation temperatures within our time scales.

As expected from its peculiar surface structure, diffusion on the chiral icosahedron occurs *via* non-trivial pathways, which are markedly different from those observed in the other structures. As previously discussed, there are no true edges on the chiral surface (see Fig. 1(m)), but rather what can be described as "broken" edges, since the atomic row connecting neighboring vertices contains a kink. To move from one facet to another, the adatom must slide through the broken edge *via* a sequence of multiple jump diffusion events, which will be discussed in detail below. Exchange diffusion mechanisms are never observed.

As for diffusion rates, our simulations clearly show that inter-facet diffusion by jump is faster in the chiral icosahedron than in the Mackay icosahedron, as many more diffusion events are observed within the same simulation time. On the other hand, inter-facet diffusion by exchange is faster in the tetrahedron than in the octahedron. In the following, we will quantify these differences in diffusion rates by calculating the activation barriers for jump and exchange processes on the four nanoparticle surfaces.

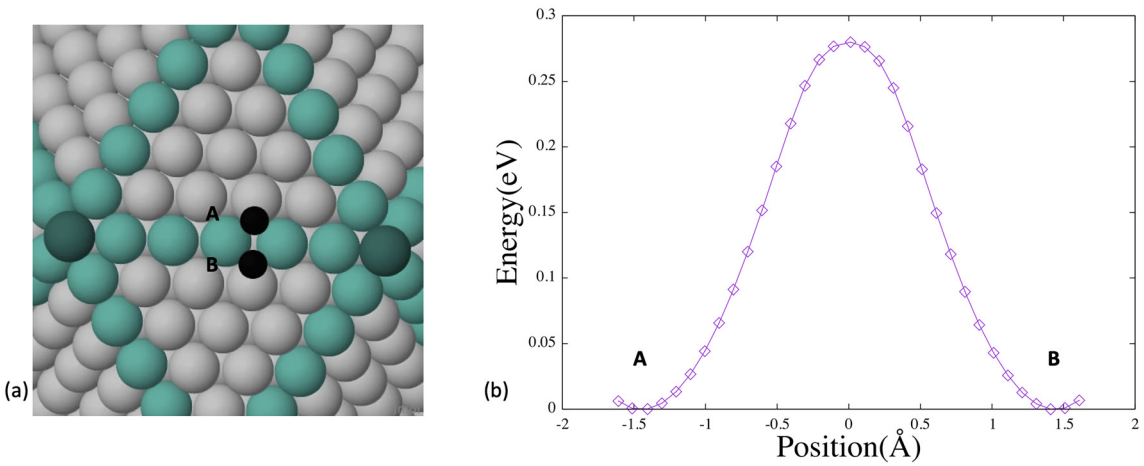

Fig. 3 Edge crossing by jump on the Mackay icosahedron. (a) Adsorption sites before and after the crossing of the edge by jump diffusion. (b) Energy profile of the diffusion process, estimated by the drag method. The energy barrier is 0.27 eV.

5 Inter-facet diffusion: edge crossing by jump

Here, we estimate the energy barriers for edge-crossing processes by jump diffusion on the different nanoparticle surfaces using the drag method. We begin by considering the Mackay icosahedron. The adatom moves from site A to site B in Fig. 3(a), crossing the edge with a single jump. Sites A and B are the three-fold hcp adsorption sites closest to the edge, located on the two adjacent facets. The saddle point corresponds to a bridge site, in which the adatom is coordinated with two edge atoms. The energy profile is shown in Fig. 3(b). The barrier is regular and symmetric, and has a height of 0.27 eV.

The inter-facet diffusion process on the chiral surface is much more complex. In Fig. 4(a), we show the diffusion pathway observed in our MD simulations, which connects five locally stable adsorption sites. At the beginning of the process, the adatom is located near the vertex on the left, on the top facet in the figure. It then progressively moves rightward, parallel to the broken edge. At the end of the process, the atom reaches the bottom facet, near the right vertex. From there, it can easily diffuse within the facet. This is the only inter-facet diffusion process observed in our simulations. Other pathways —for example, those in which the adatom moves nearly perpendicular to the edge—are never observed, and are therefore expected to be associated with higher energy barriers.

The energy profile of the multi-step process shown in Fig. 4(a) is presented in Fig. 4(b). Local minima are separated by energy barriers in the range of 0.12–0.15 eV. The highest of these barriers—located in the middle of the pathway, at the breach—is 0.15 eV, which is significantly lower than the energy barrier for the single-step edge-crossing diffusion on the Mackay icosahedral surface.

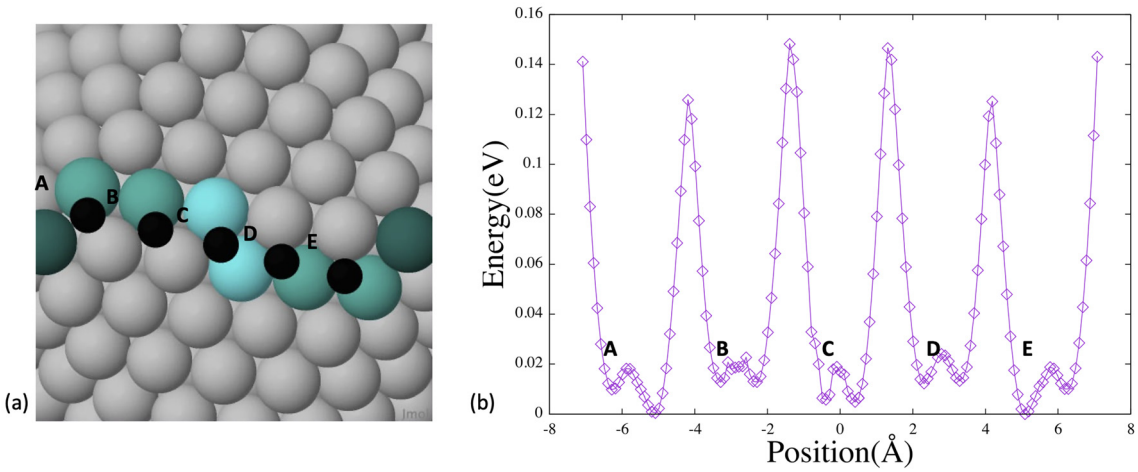

Fig. 4 Edge crossing by jump on the chiral icosahedron. (a) Locally stable adsorption sites along the inter-facet diffusion process. (b) Energy profile of the diffusion process, estimated by the drag method. The energy barrier for inter-facet diffusion is the highest among the barriers of the subsequent jump diffusion steps, *i.e.* 0.15 eV.

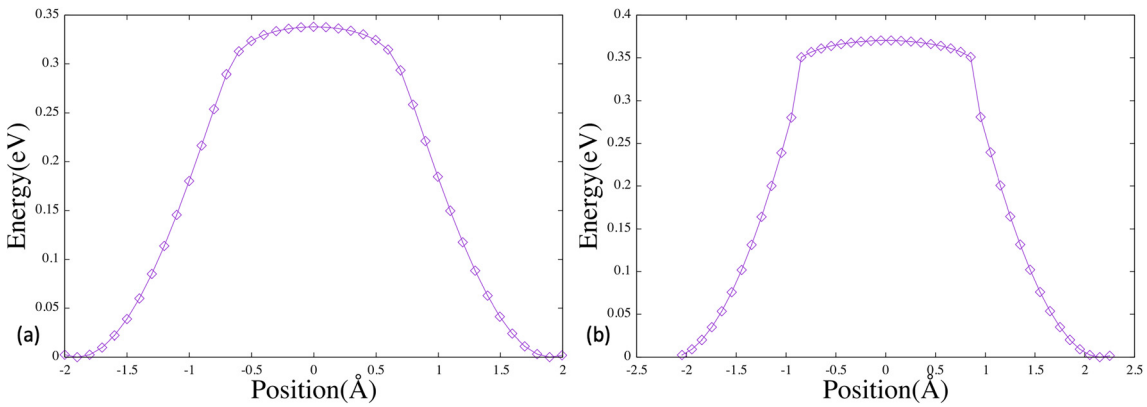

Fig. 5 Edge crossing by jump on the octahedron and tetrahedron. Energy profiles for edge crossing diffusion by jump on the (a) octahedron and (b) tetrahedron, estimated by the drag method. The energy barriers are 0.33 and 0.38 eV, respectively.

We note that, differently from the other structures, the chiral icosahedron is not purely made of Ag, but contains a Ni core, is essential to stabilize the chiral Ag surface.[35] To minimize the influence of the Ni core on surface properties, we deliberately included two full Ag layers. This ensures that Ag atoms in the outermost layer are coordinated only with other Ag atoms—thus mimicking the surface environment of a pure Ag nanoparticle. To verify that the presence of the Ni core does not affect adatom diffusion, we have calculated static diffusion barriers on a Ni@Ag structure with one more chiral Ag layer, finding the same values.

Even though inter-facet diffusion by jump is never observed on the octahedron and tetrahedron in our MD simulations, we calculate the energy barriers for such processes, which turn out to be 0.33 and 0.38 eV, respectively (see Fig. 5).

In summary, our results show that the energy barrier for inter-facet diffusion by jump strongly depends on the geometric shape of the nanoparticle: it is highest for the structure with the sharpest edge (the tetrahedron), and decreases for structures with increasingly wider edges (in order: the octahedron and the Mackay icosahedron), which can be climbed more easily by the diffusing adatom. The lowest barrier is found for the chiral icosahedron, where no true edge is present—thus representing the smoothest surface for jump diffusion.

6 Edge crossing by exchange

Here, we consider the other possible mechanism for diffusion between adjacent facets observed in our MD simulations: the exchange process. In this case, we can no longer refer to *adatom diffusion*, since the atom diffusing on the second facet is not the same as the one diffusing on the first. However, exchange processes enable *mass diffusion*, which is dynamically equivalent to adatom diffusion, provided that the nanoparticle surface and the diffusing atom are of the same species.

We do not consider the chiral icosahedron in this case, as exchange processes are never observed in the simulations and are difficult to predict due to the absence of well-defined edges.

On the Mackay icosahedron, exchange diffusion occurs *via* two different mechanisms, as shown in Fig. 6. In the first case (Fig. 6(a)), a single substitution occurs at the edge of the nanoparticle. In the second case, the process is more complex, involving two different edges and a chain of atoms in between[54] (Fig. 6(b)). The energy barrier is calculated to be 0.46 eV in the first case and 0.54 eV in the second. These values are significantly higher than the barrier for edge crossing by jump on the same surface. Indeed, jump processes are much more frequent in MD simulations, while exchange processes are only observed at the highest simulation temperatures.

Energy barriers for edge crossing by exchange are also calculated for the octahedron and the tetrahedron. In the MD simulations, we observe that exchange processes often occur near the vertices (or near the missing vertices, in the case of the tetrahedron), suggesting that exchange is more favorable at these positions than elsewhere along the edge. Indeed, the barrier for exchange near the vertex is 0.13 eV for the octahedron, while it is much higher (0.31 eV) when the exchange takes place at other edge sites. We note that, when moving from the vertex toward the center of the edge, the diffusion barrier increases sharply toward its maximum value.

On the tetrahedron, all calculated barriers are very low and comparable to those for jump diffusion on the nanoparticle facet. Diffusion near the (missing) vertex is slightly more favorable than at other positions along the edge, with energy barriers of 0.04 and 0.06 eV, respectively. Snapshots of edge cross-

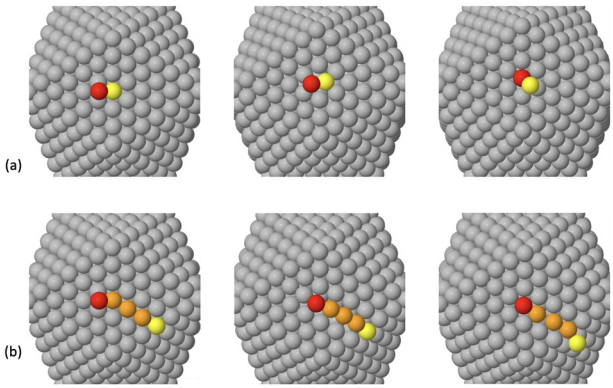

Fig. 6 Mass diffusion by exchange on the Mackay icosahedron. (a) Simple process, with two atoms involved: the adatom (in red in the figure) and one atom initially belonging to the edge (in yellow). The adatom takes the place of the edge atom, which becomes an adatom on the adjacent facet. (b) More complex process, involving many atoms: the adatom (in red), an edge atom in the opposite edge of the adjacent facet (in yellow) and a row of atoms between them (in orange). Orange atoms are pushed away by the red atom, and the yellow atom becomes and adatom on the bottom left icosahedral facet.

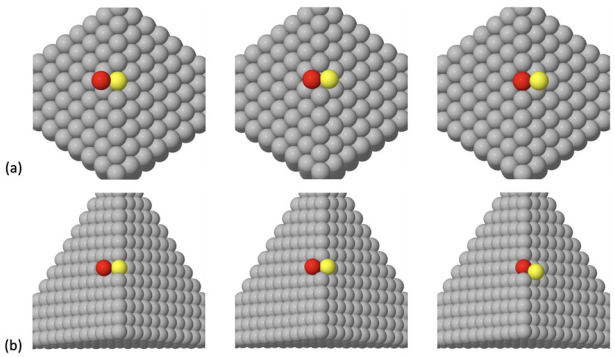

Fig. 7 Mass diffusion by exchange on the octahedron and tetrahedron. Adatom on the facet of the (a) octahedron and (b) tetrahedron is coloured in red. The adatom takes the place of one of the edge atoms (in yellow), which becomes an adatom on the adjacent facet.

ing by exchange on the octahedron and tetrahedron are shown in Fig. 7.

As with inter-facet adatom diffusion by jump, we find that the energetics of mass diffusion by exchange strongly depend on the nanoparticle shape. However, in this case, the process is more favorable in nanoparticles with sharper edges, where atoms are more weakly coordinated and can be more easily displaced and replaced by the diffusing atom. Accordingly, the most favorable structure is the tetrahedron, followed by the octahedron; in the icosahedron, exchange diffusion is much less favorable than in the other structures.

Here we want to shortly comment on the values of the energy barrier calculated by the drag method. This method provides highly precise numerical values within the framework of the chosen potential; therefore, the absolute accuracy of these barriers is limited by the reliability of the Gupta potential itself. However, this model has been extensively validated and is known to produce results in good agreement with both experimental data and more advanced calculations, particularly for silver.[25] In addition, we note that our study does not aim to provide absolute energy barriers with high precision. Rather, our goal is to compare diffusion barriers across different processes and nanoparticle geometries in order to identify systematic trends and establish a relative ranking.

Table 1 Inter-facet diffusion events in constant temperature MD simulations. Number of inter-facet diffusion events by jump on the chiral and Mackay icosahedral surface, in constant temperature MD simulations

	f (events/200 ns)	
T (K)	Chiral	Mackay
275	25	—
300	28	—
325	48	—
350	82	6
375	117	17
400	153	22
425	—	43
450	—	53

7 Dynamical energy barriers

To validate our findings, we estimate the energy barriers for inter-facet diffusion and edge crossing using an Arrhenius plot. We assume that the rate (f) of edge-crossing events depends on the temperature (T) *via* the Arrhenius law, *i.e.*, $f = A\exp\left(-\frac{\Delta E}{k_B T}\right)$, where ΔE is the energy barrier and A is a temperature-independent pre-exponential factor. For each nanoparticle shape, we perform MD simulations at different temperatures and count the number of edge-crossing events occurring within a fixed time interval of 200 ns, from which we estimate the temperature-dependent rate of such events.

If a disruptive event occurs during a simulation (*e.g.*, the detachment of a vertex atom that binds to the adatom to form a dimer), the simulation is stopped and a new one is launched, until a total simulation time of 200 ns is accumulated.

First, we compare jump diffusion mobility on the chiral and Mackay icosahedra. Our results, summarized in Table 1, show that adatom mobility is much higher on the chiral surface. For example, 82 diffusion events are recorded at 350 K on the chiral icosahedron, whereas at the same temperature, only 6 diffusion events occur on the Mackay icosahedron. At lower temperatures (275–325 K), no edge-crossing events are observed on the Mackay surface within the simulation time, with the adatom remaining trapped in the initial facet; at these same temperatures, inter-facet diffusion is already activated on the chiral surface. The data in Table 1 are used to construct the Arrhenius plot ($\ln(f)$*vs.*$1/T$), as shown in the graphs in Fig. 8. The linear fit matches our data well, especially for diffusion on the chiral surface, where many events are observed within the simulation time. Energy barriers extracted from the fits are ΔE = (0.16 ± 0.01) eV for jump diffusion on the chiral icosahedron, and ΔE = (0.28 ± 0.03) eV for the

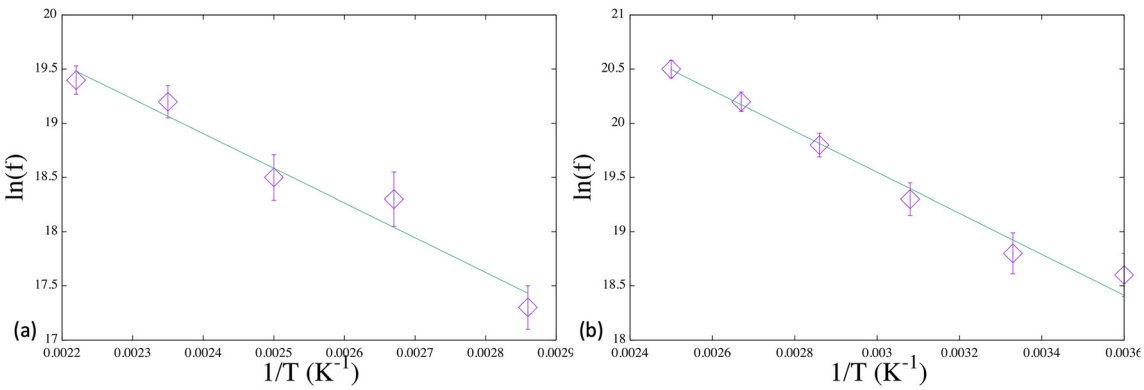

Fig. 8 Arrhenius plot for inter-facet diffusion by jump on the Mackay and chiral icosahedron. (a) Mackay icosahedron. Energy barrier and pre-exponential factor are ΔE = (0.28 ± 0.03) eV and A = 3.6 × 10^{11}. (b) Chiral icosahedron. Energy barrier and pre-exponential factor are ΔE = (0.16 ± 0.01) eV and A = 9 × 10^{10}. Frequencies f are in s^{-1}.

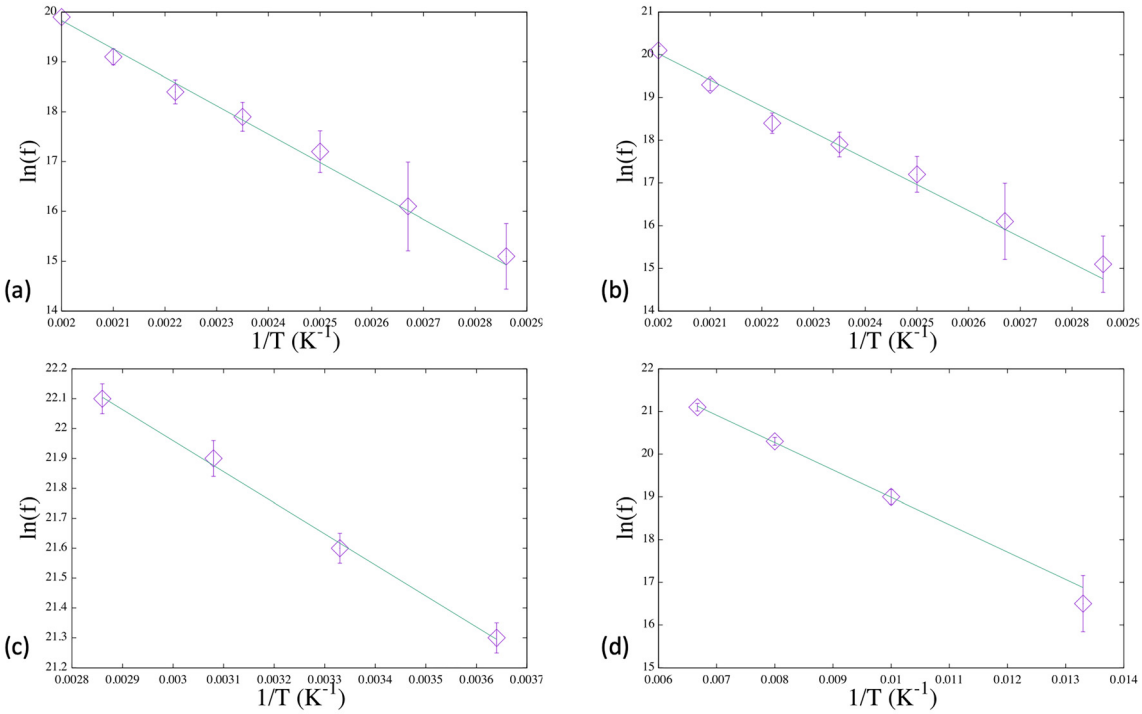

Fig. 9 Arrhenius plot for inter-facet diffusion by exchange on the Mackay, octahedron and tetrahedron. (a) Mackay icosahedron, simple exchange process (see Fig. 6(a)). Energy barrier and pre-exponential factor are ΔE = (0.40 ± 0.02) eV and A = 3.7 × 10^{13} s^{-1}. (b) Mackay icosahedron, many atom exchange process. Energy barrier and pre-exponential factor are ΔE = (0.53 ± 0.03) eV and A = 1.0 × 10^{14} s^{-1}. (c) Octahedron. Energy barrier and pre-exponential factor are ΔE = (0.09 ± 0.01) eV and A = 7.9 × 10^{10} s^{-1}. (d) Tetrahedron. Energy barrier and pre-exponential factor are ΔE = (0.06 ± 0.01) eV and A = 1.1 × 10^{11} s^{-1}. Frequencies f are in s^{-1}.

Mackay icosahedron—both in good agreement with the static energy barriers calculated using the drag method.

Using the same approach, we evaluate energy barriers for inter-facet diffusion by exchange on the Mackay icosahedron (see Fig. 9(a and b)). The results are ΔE = (0.49 ± 0.02) eV when only simple processes are considered (see Fig. 6(a)), and ΔE = (0.53 ± 0.03) eV when more complex exchanges involving multiple atoms are also included. Again, the agreement with the static energy barriers is good.

In the case of the octahedron and tetrahedron, only exchange processes occur in our MD simulations, as inter-facet diffusion by jump is highly unfavorable. Therefore, only exchange energy barriers can be estimated using the Arrhenius plot. The energy barrier for edge crossing on the octahedral surface is slightly lower than that calculated by the drag method (0.09 eV compared to 0.13 eV). This discrepancy between the two methods can be explained by closely examining the inter-facet diffusion process. To move from one facet to another, the adatom must first reach the edge *via* a sequence of intra-facet jump diffusion events; then, it crosses the edge through a single inter-facet diffusion step.

In the cases analyzed so far, edge-crossing energy barriers are much higher than those associated with intra-facet diffusion, so the inter-facet diffusion rate is dominated by a single step with the highest energy barrier—namely, edge crossing. The low-barrier diffusion steps preceding the crossing mainly influence the pre-exponential factor in the Arrhenius relation. However, on the octahedral surface, this approximation no longer holds, as the energy barriers for edge crossing by exchange are very close to those for jump diffusion on the (111) surface. Therefore, even though our data are well fitted by a linear interpolation (see Fig. 9(c)), the estimated energy barrier represents an effective barrier for the entire diffusion process, which includes both edge-approach and edge-crossing events. The value lies between the barriers of the two distinct steps (0.06 and 0.13 eV, as estimated by the drag method).

The same considerations apply to inter-facet diffusion on the tetrahedral surface. However, in this case, intra-facet jump diffusion and edge crossing by exchange have almost the same energy barriers (0.04–0.06 eV, as estimated by the drag method). The effective energy barrier obtained from the Arrhenius plot is also ΔE = (0.06 ± 0.01) eV.

8 Conclusions

In this work, we have studied the mobility of a silver adatom on nanoparticles with silver surface and with different geometric shapes—namely, the tetrahedron, octahedron, Mackay icosahedron, and chiral icosahedron. All considered nanoparticles expose close-packed (111) surfaces and differ only in

the types of edges that separate adjacent facets. Our results demonstrate that the nanoparticle shape strongly affects adatom mobility and, specifically, that the edge type determines which inter-facet diffusion processes are more favorable and what the associated activation barriers are.

The estimated energy barriers for the various edge-crossing processes on the different nanoparticle surfaces are summarized in Table 2. These values allow us to establish a "ranking" of nanoparticle shapes in terms of smoothness, *i.e.*, the ease with which an adatom of the same chemical species diffuses over their surface.

If we consider only jump processes—where the adatom moves from one facet to an adjacent one by climbing the separating edge—the smoothest shape is the chiral icosahedron, followed by the Mackay icosahedron, the octahedron, and the tetrahedron. In this case, the ranking reflects the sharpness of the edges: mobility is more hindered when the edge is sharper. The chiral icosahedron, in which no true edge exists, is the smoothest structure for jump diffusion.

The energy barriers for exchange processes—where the adatom enters the edge, replacing another atom that is then pushed onto the adjacent facet—show the opposite trend. Exchange is facilitated when the edge is sharper, *i.e.*, when edge atoms are less coordinated and can therefore be more easily displaced. As such, the smoothest surface for exchange diffusion is that of the tetrahedron, followed by the octahedron and the Mackay icosahedron. Exchange processes are never observed in the chiral icosahedron, where all surface atoms are highly coordinated.

When considering both diffusion mechanisms, the nanoparticle shapes can be ranked in terms of smoothness as follows: tetrahedron, chiral icosahedron, octahedron, and Mackay icosahedron. This result agrees with recent computational studies on metal nanoparticle growth, which show that tetrahedra and chiral icosahedra grow particularly well, forming structures with very few surface defects even at relatively large sizes.[24,35] In other words, tetrahedra and chiral icosahedra behave more similarly to extended 2D surfaces during growth. Very smooth shell-by-shell growth is expected when atoms are deposited on nanoparticles with these shapes, analogous to the layer-by-layer growth observed in thin films.

Adatom mobility on nanoparticles is primarily influenced by the geometric features of their surfaces. We therefore expect our results to hold for other fcc metals as well (such as Au, Cu, Pt, and Pd), which exhibit the same types of nanoparticle structures as Ag. Specifically, we expect that the relative ordering of energy barriers for jump and exchange inter-facet diffusion across the different nanoparticle shapes would be similar to what we observed for Ag, while of course the magnitude of the barriers would be affected by the bond strength of the different metals.

We note that, in the case of homo-diffusion (where the surface and the diffusing atom are of the same species), jump and exchange processes are equivalent, as both result in mass transport from one facet to another. This is not the case for hetero-diffusion, where the surface atoms and the adatom belong to different chemical species. In this case, jump and exchange processes have different outcomes: if edge crossing occurs *via* a jump, the adatom retains its original chemical identity; by contrast, an exchange process results in the incorporation of a surface atom as the new adatom, initiating a homo-diffusion process. Therefore, in hetero-diffusion, only jump processes contribute to the migration of the foreign species, making the icosahedral shapes—especially the chiral icosahedron—the smoothest surfaces for diffusion.

This work contributes to the broader understanding of nanoparticle growth. Nanoparticle growth is a highly complex phenomenon, influenced by a wide range of additional factors. These include the diffusion of small atomic clusters—generally less mobile than single adatoms—the formation of surface defects during growth, which may act as trapping sites, and the presence of facets with different crystallographic orientations, such as (100) or (110).[55] All these effects are essential for a complete modeling of growth dynamics. Here, we have deliberately focused on defect-free nanoparticles with only (111) facets, for a clean and controlled comparison of edge types across different polyhedral shapes. By clarifying the specific role of edge geometry in adatom diffusion, our work offers insights that can inform more comprehensive growth models and may help to interpret shape selection mechanisms observed in experiments.

A natural perspective of this work is to apply the same methodology to investigate the effect of nanoparticle geometric shape on hetero-diffusion, which is particularly relevant for the growth of bimetallic nanoparticles. Besides the already cited case in which the nanoparticle and the diffusing adatom belong to two different chemical species, an equally interesting class of systems involves nanoparticles whose surfaces are composed of two atomic species—for instance, with different species preferentially occupying inequivalent surface sites.[56] These systems offer exciting possibilities for tuning surface

Table 2 Energy barriers for inter-facet diffusion on Ag nanoparticles. Summary of our results for inter-facet diffusion barriers on Ag nanoparticles with closed-packed (111) surface. Energy barriers in the Table have been calculated by the drag method, but are in agreement with dynamical barriers estimated by the Arrhenius plot

Structure	Edge-crossing process		Energy barrier (eV)
Mackay icosahedron	Jump		0.28
	Exchange	2 atoms	0.46
		Many atoms	0.52–0.54
Chiral icosahedron	Jump		0.15
Octahedron	Jump		0.33
	Exchange	Edge center	0.31
		Near vertices	0.13
Tetrahedron	Jump		0.38
	Exchange	Edge center	0.06
		Near (removed) vertices	0.04

diffusion and growth mechanisms through compositional design.

Author contributions

N. C. performed and analyzed molecular dynamics simulations and performed energy barrier calculations. R. F. and D. N. conceptualized and supervised the work, and wrote the original draft of the paper. All authors approved the final version of the paper.

Conflicts of interest

There are no conflicts to declare.

Data availability

Data for this article, including the code for molecular dynamics simulations, are available at **https://doi.org/10.5281/zenodo.15302720**.

Acknowledgements

The authors acknowledge financial support under the National Recovery and Resilience Plan (NRRP), Mission 4, Component 2, Investment 1.1, Call for tender no. 104 published on 2.2.2022 by the Italian Ministry of University and Research (MUR), funded by the European Union – NextGenerationEU– Project Title PINENUT – CUP D53D23002340006 – Grant Assignment Decree No. 957 adopted on 30/06/2023 by the Italian Ministry of University and Research (MUR). The authors acknowledge networking support from the IRN Nanoalloys of CNRS.

References

1 H. Brune, *Surf. Sci. Rep.*, 1998, **31**, 125–229.
2 N. Kaiser, *Appl. Opt.*, 2002, **41**, 3053–3060.
3 T. Ala-Nissila, R. Ferrando and S. C. Ying, *Adv. Phys.*, 2002, **51**, 949–1078.
4 G. Kellogg and P. J. Feibelman, *Phys. Rev. Lett.*, 1990, **64**, 3143.
5 R. Stumpf and M. Scheffler, *Phys. Rev. B:Condens. Matter Mater. Phys.*, 1996, **53**, 4958–4973.
6 E. Elkoraychy, K. Sbiaai, M. Mazroui, Y. Boughaleb and R. Ferrando, *Surf. Sci.*, 2015, **635**, 64–69.
7 P. J. Feibelman, *Phys. Rev. B:Condens. Matter Mater. Phys.*, 2001, **64**, 125403.
8 F. Montalenti and R. Ferrando, *Phys. Rev. B:Condens. Matter Mater. Phys.*, 1998, **58**, 3617–3620.
9 H. Bulou and C. Massobrio, *Phys. Rev. B:Condens. Matter Mater. Phys.*, 2005, **72**, 205427.
10 A. Bogicevic, J. Strömquist and B. I. Lundqvist, *Phys. Rev. Lett.*, 1998, **81**, 637–640.
11 O. M. Braun and R. Ferrando, *Phys. Rev. E:Stat., Nonlinear, Soft Matter Phys.*, 2002, **65**, 061107.
12 M. Villarba and H. Jónsson, *Surf. Sci.*, 1994, **317**, 15–36.
13 J. Merikoski and T. Ala-Nissila, *Phys. Rev. B:Condens. Matter Mater. Phys.*, 1995, **52**, R8715–R8720.
14 J. Merikoski, I. Vattulainen, J. Heinonen and T. Ala-Nissila, *Surf. Sci.*, 1997, **387**, 167–182.
15 F. Montalenti and R. Ferrando, *Phys. Rev. B:Condens. Matter Mater. Phys.*, 1999, **59**, 5881–5891.
16 G. Antczak and G. Ehrlich, *Surf. Sci. Rep.*, 2007, **62**, 39–61.
17 M. Jäckle and A. Groß, *J. Chem. Phys.*, 2014, **141**, 174710.
18 M. Jäckle, K. Helmbrecht, M. Smits, D. Stottmeister and A. Groß, *Energy Environ. Sci.*, 2018, **11**, 3400–3407.
19 D. Gaissmaier, D. Fantauzzi and T. Jacob, *J. Chem. Phys.*, 2018, **150**, 041723.
20 F. Hontinfinde, R. Ferrando and A. Levi, *Surf. Sci.*, 1996, **366**, 306–316.
21 M. Benlattar, E. El koraychy, A. Kotri and M. Mazroui, *Eur. Phys. J. Plus*, 2017, **132**, 522.
22 E. Seebauer and C. Allen, *Prog. Surf. Sci.*, 1995, **49**, 265–330.
23 K. Wegner, P. Piseri, H. V. Tafreshi and P. Milani, *J. Phys. D: Appl. Phys.*, 2006, **39**, R439.
24 Y. Xia, D. Nelli, R. Ferrando, J. Yuan and Z. Y. Li, *Nat. Commun.*, 2021, **12**, 3019.
25 D. Nelli, C. Roncaglia, R. Ferrando, Z. Kataya, Y. Garreau, A. Coati, C. Andreazza-Vignolle and P. Andreazza, *Nanoscale*, 2023, **15**, 18891–18900.
26 F. Baletto, C. Mottet and R. Ferrando, *Surf. Sci.*, 2000, **446**, 31–45.
27 J. Yang, W. Hu, Y. Wu and X. Dai, *Cryst. Growth Des.*, 2012, **12**, 2978–2985.
28 X. Xia, S. Xie, M. Liu, H.-C. Peng, N. Lu, J. Wang, M. J. Kim and Y. Xia, *Proc. Natl. Acad. Sci. U. S. A.*, 2013, **110**, 6669–6673.
29 R. G. Weiner, C. J. DeSantis, M. B. T. Cardoso and S. E. Skrabalak, *ACS Nano*, 2014, **8**, 8625–8635.
30 M. Gao, D. Wen, G. Cao, Y. Zhang, Y. Deng and J. Hu, *Appl. Surf. Sci.*, 2023, **640**, 158286.
31 J. Yang, W. Hu, S. Chen and J. Tang, *J. Phys. Chem. C*, 2009, **113**, 21501–21505.
32 J. Yang, W. Hu, Y. Wu and X. Dai, *Surf. Sci.*, 2012, **606**, 971–980.
33 X. Dai, J. Yang, W. Hu, Z. Yang and S. Peng, *Int. J. Mod. Phys. B*, 2020, **34**, 2050015.
34 X. Dai, C. Zhu, D. Wen and W. Hu, *Thin Solid Films*, 2021, **737**, 138938.
35 N. Canestrari, D. Nelli and R. Ferrando, *Nat. Commun.*, 2025, **16**, 1655.
36 A. L. Mackay, *Acta Crystallogr.*, 1962, **15**, 916–918.
37 V. Rosato, M. Guillope and B. Legrand, *Phil. Mag. A*, 1989, **59**(2), 321–336.
38 R. P. Gupta, *Phys. Rev. B:Condens. Matter Mater. Phys.*, 1981, **23**, 6265.

39 F. Baletto, C. Mottet and R. Ferrando, *Phys. Rev. B:Condens. Matter Mater. Phys.*, 2002, **66**, 155420.
40 F. Baletto, C. Mottet and R. Ferrando, *Phys. Rev. Lett.*, 2003, **90**, 135504.
41 R. Ferrando and G. Tréglia, *Surf. Sci.*, 1995, **331–333**, 920–924.
42 M. Langelaar, M. Breeman and D. Boerma, *Surf. Sci.*, 1996, **352–354**, 597–601.
43 L. Bardotti, M. C. Bartelt, C. J. Jenks, C. R. Stoldt, J.-M. Wen, C.-M. Zhang, P. A. Thiel and J. W. Evans, *Langmuir*, 1998, **14**, 1487–1492.
44 J. Paez-Ornelas, H. Fernández-Escamilla, N. Takeuchi and J. Guerrero-Sánchez, *Mater. Today Commun.*, 2020, **25**, 101461.
45 G. Boisvert and L. J. Lewis, *Phys. Rev. B:Condens. Matter Mater. Phys.*, 1996, **54**, 2880–2889.
46 H. Brune, K. Bromann, H. Röder, K. Kern, J. Jacobsen, P. Stoltze, K. Jacobsen and J. Norskov, *Phys. Rev. B:Condens. Matter Mater. Phys.*, 1995, **52**, R14380–R14383.
47 C. Ratsch, A. P. Seitsonen and M. Scheffler, *Phys. Rev. B: Condens. Matter Mater. Phys.*, 1997, **55**, 6750–6753.
48 D. Nelli, A. Krishnadas, R. Ferrando and C. Minnai, *J. Phys. Chem. C*, 2020, **124**, 14338–14349.
49 D. M. Wells, G. Rossi, R. Ferrando and R. E. Palmer, *Nanoscale*, 2015, **7**, 6498–6504.
50 G. Henkelman, G. Jóhannesson and H. Jónsson, in *Methods for Finding Saddle Points and Minimum Energy Paths*, ed. S. D. Schwartz, Springer Netherlands, Dordrecht, 2002, pp. 269–302.
51 C. H. Bennett, in *Diffusion in Solids: Recent*, ed. A. S. Nowick and J. J. Burton, Academic Press, New York, 1975.
52 J. Nocedal and S. J. Wright, *Numerical Optimization*, Springer, 2nd edn, 2006.
53 D. Nelli, V. Mastronardi, R. Brescia, P. P. Pompa, M. Moglianetti and R. Ferrando, *Nano Lett.*, 2023, **23**, 2644–2650.
54 M. Rocca, T. Rahman and L. Vattuone, *Springer handbook of surface science*, Springer Nature, 2021.
55 J. Zhao, E. Baibuz, J. Vernieres, P. Grammatikopoulos, V. Jansson, M. Nagel, S. Steinhauer, M. Sowwan, A. Kuronen, K. Nordlund and F. Djurabekova, *ACS Nano*, 2016, **10**, 4684–4694.
56 P. Grammatikopoulos, J. Kioseoglou, A. Galea, J. Vernieres, M. Benelmekki, R. E. Diaz and M. Sowwan, *Nanoscale*, 2016, **8**, 9780–9790.